Free space optical beam coupled to surface plasmonic polariton waves via designed grooves in metal film

Yuegang Chen (陈跃刚)[1,2] and Zhiyuan Li (李志远)[2,*]

[1]*Department of Physics, Guizhou University, Guiyang 550025, China*
[2]*Laboratory of Optical Physics, Institute of Physics, Chinese Academy of Science, Beijing 100190, China*
**Corresponding author: lizy@aphy.iphy.ac.cn*

Received September 1, 2014; accepted November 28, 2014; posted online February 9, 2015

Surface plasmonic polariton (SPP) waves with complicated wavefronts have important implications in nanophotonic sciences and applications. The surface electromagnetic wave holography method is applied to designed grooves on a metal surface for coupling a plane wave in free space to complicated wavefront SPP waves. The grooves illuminated by the plane wave incident from free space serve as secondary SPP waves sources, that radiate cylindrical SPP waves. New controllable wavefronts originate from these secondary SPP waves interfering with each other, based on the Huygens–Fresnel principle. Several applications of the method are demonstrated, such as converting coupling waves in free space into focusing SPP waves on a metal surface.

OCIS codes: 050.1970, 240.6680, 310.6628.
doi: 10.3788/COL201513.020501.

Surface plasmonic polariton (SPP) waves are collective resonances of electron gas in a metal surface. They have the unique properties of strong confinement of light energy to the sub-wavelength scale, and large enhancement of the local field intensity[1–4]. SPPs have a wide range of applications, including nanometer optical circuits[5,6], solar cells[7], enhanced fluorescence[8] and Raman spectroscopy[9], and sensors[10]. Many plasmonic structures have been proposed to achieve the excitation[11,12], unidirectional launching[13,14], and focusing of SPP waves[15–17].

To excite SPP waves on a flat metal surface, an excess wave vector is required, since the wave vector of SPP waves is greater than the vector in free space. Prism coupling is a primary method to match the wave vector[1,18]. In this method, the prism produces an evanescent wave to match the wave vector through total internal reflection. The periodical grating etched on a metal surface can couple waves in free space into SPP waves through the Bragg vector, which supplies the excess vector[1].

The above-mentioned methods only apply to the excitation of simple wavefront SPP waves. More extensive applications are needed for more complicated wavefront SPP waves. Recently, a few methods have been proposed to generate complicated wavefront SPP waves. Nanometer particles and holes arranged on a simple circular arc array can excite SPP waves by scattering the light incident from free space and focusing them on the destination using constructive interference[19]. A non-periodic nanoslit array is designed by the simulated annealing method and applied to couple free-space light into SPP waves and simultaneously focus SPP waves of varying wavelengths onto various predefined locations[20]. An SPP wavefront-shaping method is proposed[21]. In this method, the Fourier transform of the desired wavefront is encoded into the spatial frequency of a grating. Then, the incident SPP waves or free-space beams are modulated by the grating to realize shaping of the wavefront. This demands the mathematical expression of desired wavefront and the following Fourier transform.

However, a direct and simple method is still highly desirable for the design of nanostructures to excite and control complicated wavefront SPP waves on a metal surface. Recently, the surface wave holography (SWH) methodology has been proposed to design complicated groove patterns for shaping the SPP waves' radiation from the metal surface. With the SWH method, various wavefront shaping functionalities such as arbitrary single-point focusing, single-direction beam collimation, two-point focusing, and complicated pattern imaging in free space can be achieved[22,23]. The method has also been employed to control SPP waves propagating on metal surface[24,25]. In this Letter, we apply the SWH method to design plasmonic nanostructures to couple the plane wave in free space to complicated wavefront SPP waves on a metal surface, for instance, we focus SPP waves and SPP waves that are compatible with the modal profile of an SPP waveguide.

In the framework of the SWH method[22–25], a series of complicated grooves etched on the surface of a metal film are applied to scatter the incident wave and excite the SPP waves on the metal surface. Every groove point is regarded as the source of secondary SPP waves. According to the Huygens–Fresnel principle, the coherent superposition of these secondary SPP waves determines the wavefronts of SPP waves. Therefore, the groove patterns need be designed deliberately so that the SPP waves interfere to produce the desired wavefronts. The SWH method includes a writing and reading process. In the writing process, the reference wave is a wave with the complex amplitude $U_W = A_W(x, y)\exp[-i\psi_W(x, y)]$ incident

on the metal surface. An object on a metal surface radiates SPPs on a metal surface with the amplitude $U_O = A_O(x, y)\exp[-i\psi_O(x, y) - i\varphi_0]$. In the computer designing work, the object wave U_O interferes with the reference wave U_W. The intensity distribution of the interference pattern on the metal film is $I_1 = (U_W + U_O)(U_W + U_O)^*$. The maxima occur at

$$\psi_O - \psi_W + \varphi_0 = 2m\pi, \tag{1}$$

where $m = 0, \pm1, \pm2, \ldots$ is the integer. Grooves are etched at these maximal positions, leaving the rest flat. It must be considered that the lateral scale of the grooves are much smaller than the wavelength, typically $\lambda/10$. The discrete approximation can be introduced by using a δ function to express the groove's effect on the scatter source. The hologram corresponding to λ is obtained by the following:

$$H(x, y) = \alpha\sum_m \delta(\psi_O - \psi_W + \varphi_0 = 2m\pi). \tag{2}$$

The groove patterns are designed by the SWH method through computer calculations. In the actual implementation, the groove patterns are transferred to a metal surface using focused ion beam lithography.

In the reading process shown in Fig. 1(b), a reconstruction wave that is the same as the reference wave in the writing process illuminates the groove region and is scattered by the grooves. The scattered waves interfere constructively, and the object wave can be reproduced.

In the first example of the design by the SWH method, a free-space plane wave with an optical beam incident on the metal surface is intended to excite a focusing SPP wave via specific holographic groove patterns. The morphologies of the groove patterns must be determined by us using the SWH methodology. During the writing process, in order to obtain a focused SPP wave on the metal surface, a point O at $\mathbf{r}_0$ ($x_0 = 0$, $y_0 = -8$ μm) on metal surface (xy plane with $z = 0$) is selected as the object. A cylindrical wave originating from the point of O radiates on the metal surface, carrying the object information with the complex amplitude $U_O = (A_O/\sqrt{|\mathbf{r} - \mathbf{r}_0|})\exp\{-i[k_{\mathrm{SP}}(|\mathbf{r} - \mathbf{r}_0|) + \varphi_0]\}$. Here, k_{SP} is the wave vector of the SPP waves on the metal surface with $k_{\mathrm{SP}} = n_{\mathrm{eff}}k_0$, n_{eff} is the effective index of the SPP waves, k_0 is the wave vector in the vacuum, and A_O is the amplitude of the object wave. For the interface between the gold and the vacuum, the effective index of the SPP waves is $n_{\mathrm{eff}} = \sqrt{\varepsilon_m/(\varepsilon_m + 1)}$. Here, ε_m is metal dielectric constant. As a plane wave is intended to couple into the SPP wave that is focused on the metal surface, the corresponding reference wave is a plane wave that is incident on the metal with an incident angle of θ and the complex amplitude $U_W = A_W\exp[-i(k_0 z\cos\theta + y\sin\theta)]$. In this equation, A_W is the amplitude of the reference wave. Here, reference waves with the following three incident angles are considered: $\theta = 0°$, 15°, and 30°. The considered wavelength of the incident plane wave is $\lambda_0 = 1.064$ μm and the corresponding dielectric constant of the gold is $\varepsilon_m = -48.75 + 3.64i$. The object wave interferes with the reference wave. The intensity distribution of the interference patterns on the metal surface for the three incident angles obtained is shown in Figs. 2(a), 2(e), and 2(i) for $\theta = 0°$, 15°, and 30°, respectively. The holographic groove region is supposed to be confined within a finite space of -10 μm $< x < 10$ μm and $0 < y < 20$ μm. The holograms are obtained by etching grooves that are 0.12 μm in width at the positions of maximal intensity, with the corresponding morphology shown in Figs. 2(b), 2(f), and 2(j) for $\theta = 0°$, 15°, and 30°, respectively. The red portion represents the metal surface, and the blue slim lines represent the grooves etched on the metal surface. One can see that the groove density decreases as the incident angle increases.

Now that the holographic groove patterns have been generated, we proceed to evaluate their performance.

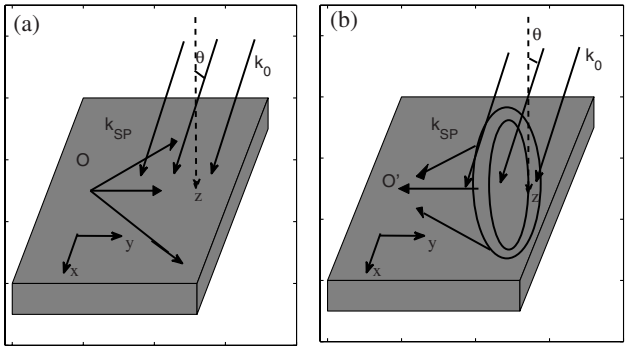

Fig. 1. Schematic of the surface electromagnetic wave hologram. (a) The writing process, where metal surface is an $x - y$ plane, (b) The reading process.

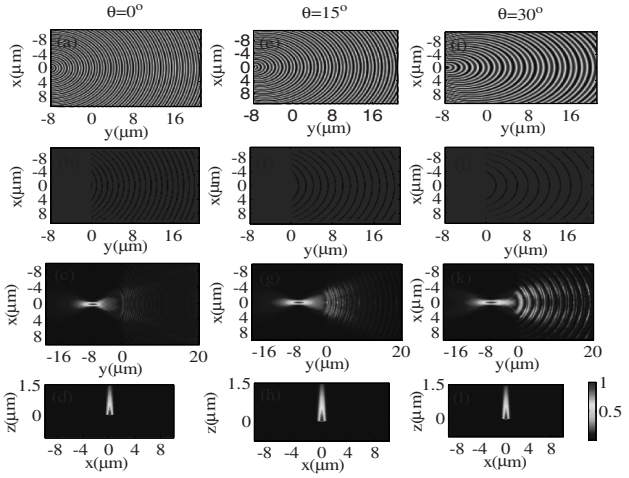

Fig. 2. Design of the groove pattern used to couple a plane wave in free space to a focusing SPP wave on a metal surface. Panels (a)–(d), (e)–(h), and (i)–(l) are for the incident angles $\theta = 0°$, $\theta = 15°$, and $\theta = 30°$, respectively. Panels (a), (e), and (i) show the interference intensity pattern, while (b), (f), and (j) show the groove pattern. (c), (g), (k), and (d), (h), (l) display the reconstruction result of the intensity distribution in the $x - y$ plane and $x - z$ plane where $y = -8$ μm, respectively.

Namely, we are examining how the pre-designated SPP wavefronts can be reconstructed in the reading process. The reading processes are simulated by the three-dimensional finite difference time-domain (3D–FDTD) method. During the reading process [shown in Fig. 1(b)], three reconstruction waves with incident angles $\theta = 0°$, 15°, and 30°, which are the same as those of reference wave in the writing process, illuminate the groove region shown in Figs. 2(b), 2(f), and 2(j), respectively. The incident wave is scattered by the grooves, and the SPP waves are excited. These SPP waves interfere constructively at the object point's original position, based on the Huygens–Fresnel principle. The SPP waves' field intensity patterns is calculated by the 3D–FDTD method. The field intensity patterns when $\theta = 0°$ are illustrated in Figs. 2(c) and 2(d), in Figs. 2(g) and 2(h) when $\theta = 15°$, and Figs. 2(k) and 2(l) when $\theta = 30°$. All grooves are of the depth of 0.08 μm. In Figs. 2(c), 2(g), and 2(k), the intensity patterns on the metal surface are shown. Obviously, the foci are reconstructed at the point where $x = 0$ and $y = -8$ μm for $\theta = 0°$, 15°, and 30°, which agrees well with the pre-designated values. In Figs. 2(d), 2(h), and 2(l), the intensity distributions in the $x - z$ plane where $y = -8$ μm are shown. Obviously, the SPP waves are well confined to the metal surface, and the off-plane scattering effect is not significant. When the incident angle $\theta = 0°$, the full widths at half-peak of the focal spots in the x and y directions are $\delta x = 0.76$ μm and $\delta y = 2.6$ μm, respectively. Above the three object points, O is reconstructed. In other words, the functionality of coupling the plane waves in free space with three incident angles to the predefined focal location O on the metal surface has been realized through such an elementary hologram.

An important parameter in measuring the performance of this plasmonic focusing device is the coupling efficiency, which is defined as the ratio of the total energy flux entering the focal area (with a cross-sectional size of 2 μm × 2 μm in the $x - z$ plane) over the total energy flux of the plane wave illuminating the groove region. The results are illustrated in Fig. 3(a), which shows a series of groove depths and the three incident angles $\theta = 0°$, 15°, and 30°. The influence of groove depth h on the coupling efficiencies can be clearly seen. When $h = 0.08$ μm, the coupling efficiencies reach the maximal values of 5.4% when $\theta = 0$ and 13.5% when $\theta = 15°$. When $\theta = 30°$, the coupling efficiency reaches the maximal value of 7.0% at $h = 0.1$ μm. These sub-wavelength grooves scatter the incident wave from free space and excite the SPP waves. The scattering effect is important for the coupling. If the depth of the groove is small, the scattering is not effective. Correspondingly, the SPP wave excitation efficiency of the groove is very low, leading to a low focal efficiency. However, if the depth of the groove is too large, the groove can capture the incident wave, due to the resonance. The excited SPPs are confined to the groove and there is a loss of energy, which also leading to a low focal efficiency. The influence of incident angle θ on the coupling efficiency is shown in Fig. 3(b). The groove depth is set as $h = 0.08$ μm. With

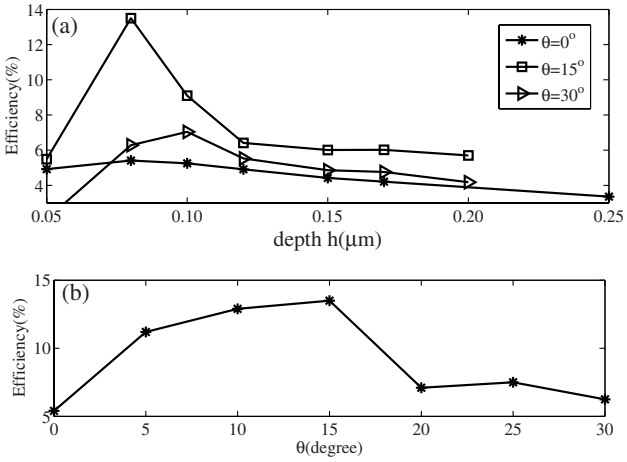

Fig. 3. Influence of groove depth and incident angle on the coupling efficiencies. (a) Groove depth h. (b) Incident angle θ.

the incident angle θ increasing, the coupling efficiency also increases, reaching the maximal value of 13.5% at $\theta = 15°$ before decreasing. The excited SPP waves propagating on the metal surface can also be scattered into free space by the grooves. For a given region, the number of groove decreases as the incident angle increases, resulting in the decrease of scattering loss. This can be seen in Figs. 2(b), 2(f), and 2(j). On the other hand, when the incident angle increases, the decreasing number of grooves will result in the reduction of the generation sources of the SPP waves. At the incident angle $\theta = 15°$, the scattering loss decrease effect balances out the SPP waves generation sources reducing effect, and the coupling efficiency reaches its maximum.

The second example of design to illustrate the power of the SWH method involves coupling an incident plane wave to dual focusing points of SPP waves via holographic groove patterns. In the writing process, two point sources, P_1 and P_2, which are located at $\mathbf{r}_1(x = -8\ \mu\text{m}, y = -2\ \mu\text{m})$ and $\mathbf{r}_2(x = -8\ \mu\text{m}, y = 2\ \mu\text{m})$, are set as the object of the SPP waves. The corresponding object wave is expressed as $U_O = (A_O/\sqrt{|\mathbf{r}-\mathbf{r}_1|})\exp\{-i[k_{\text{SP}}(|\mathbf{r}-\mathbf{r}_1|)]\} + (A_O/\sqrt{|\mathbf{r}-\mathbf{r}_2|})\exp\{-i[k_{\text{SP}}(|\mathbf{r}-\mathbf{r}_2|)]\}$. Two plane reference waves with incident angles $\theta = 0°$ and $\theta = 15°$ are considered to be incident to the metal surface and interfere with the object wave, resulting in the intensity distributions shown in Fig. 4(a) when $\theta = 0°$ and Fig. 4(e) when $\theta = 15°$. The groove region is supposed to be confined within the finite space of $-10\ \mu\text{m} < x < 10\ \mu\text{m}$ and $0 < y < 20\,\mu\text{m}$. In this area, we etch grooves of 0.08 μm in depth and 0.12 μm in width at the positions of maximal intensity. As shown in Figs. 4(b) and 4(f), a complicated groove pattern appears. In the reading process, a plane beam that is the same as the reference wave in the writing process illuminates the groove area, and the SPP waves are excited by the grooves. The field intensity patterns of the SPP waves as calculated by the 3D–FDTD method are illustrated in Figs. 4(c) and 4(d) when $\theta = 0°$ and Figs. 4(g) and 4(h) when $\theta = 15°$. Two focal spots are

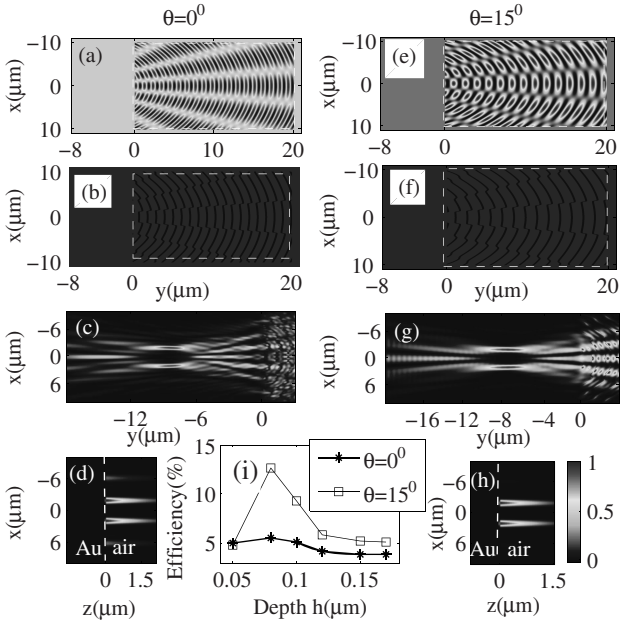

Fig. 4. Design of the groove pattern used to couple a plane wave to dual-points SPPs on a metal surface. For $\theta = 0°$, (a) is the interference intensity pattern and (b) is the groove pattern. For reconstruction intensity, (c) is the $x - y$ plane and (d) is $x - z$ plane when $y = -8$ μm. For $\theta = 15°$, (e) is the interference intensity pattern and (f) is the groove pattern. For the reconstruction intensity, (g) is the $x - y$ plane and (h) is the $x - z$ plane when $y = -8$ μm. (i) The influence of the groove depth on the coupling efficiency for $\theta = 0°$ and $\theta = 15°$.

reconstructed, with their centers located at $x = \pm 2$ μm and $y = -8$ μm when $\theta = 0°$ and $\theta = 15°$. In Figs. 4(d) and 4(h), the intensity distribution in the xz plane where $y = -8$ μm is shown. One can see that the foci at $\theta = 15°$ are better than those at $\theta = 0°$. The SPP waves are clearly confined to the metal surface when $\theta = 0°$ and $\theta = 15°$. The influences of the groove depths are considered for incident angle $\theta = 0°$ and $\theta = 15°$, as shown in Fig. 4(i). Here, the coupling efficiency is defined as the ratio of the total energy flux entering the two focal areas $-3 \le x \le -1$ and $1 \le x \le 3$ (with $-0.5 \le z \le 1.5$) over the total energy flux of the plane wave illuminating the groove region. The coupling efficiencies reach the maximal values of 5.6% and 12.6% when $\theta = 0°$ and $\theta = 15°$, respectively, when the groove depth is $h = 0.08$ μm. The optimal groove depth is the same as that of a single focal point.

The above two structures are designed to realize simple-point and dual-points focusing of the SPP waves. This can be applied to connecting optical waves in free space to elemental plasmonic devices at given positions, such as waveguides, nanoparticles, or nanoantennae on a metal surface.

In conclusion, a plane wave in free space is coupled to complicated wavefront SPP waves on a metal surface through groove patterns that are deliberately designed by the SWH method. The pre-designated functionalities of simple-point and dual-points focusing of SPP waves are realized successfully by simple holographic groove patterns that are determined easily, directly, and without the need of a complicated inverse-problem solution. These results, when combined with the previous successful applications in off-plane and in-plane wavefront shaping of SPP waves, further strongly support the SWH methodology as a universal and powerful tool for the control of SPP waves on the metal surface. The SWH method will be very useful for building novel plasmonic devices and circuits.

This work was supported by the National 973 Program of China (No. 2013CB632704), the Knowledge Innovation Program of the Chinese Academy of Sciences (No. Y1V2013L11) and the National Natural Science Foundation of China (Nos. 11374357 and 11104041).

References

1. H. Raether, *Surface Plasmons on Smooth and Rough Surfaces and on Gratings* (Springer-Verlag, 1988).
2. L. B. William, D. Alain, and T. W. Ebbesen, Nature **424**, 824 (2003).
3. M. I. Stockman, Opt. Express **19**, 22029 (2011).
4. J. F. Li, H. L. Guo, and Z. Y. Li, Photon. Res. **1**, 28 (2013).
5. S. I. Bozhevolnyi, *Plasmonic Nanoguides and Circuits* (Pan Stanford, 2008).
6. C. Ye, Y. Liu, J. Wang, H. Lv, and Z. Yu, Chin. Opt. Lett. **12**, 092402 (2014).
7. H. A. Atwater and A. Polman, Nat. Mater. **9**, 205 (2010).
8. S. Y. Liu, L. Huang, J. F. Li, C. Wang, Z. M. Meng, Z. Shi, and Z. Y. Li, J. Phys. Chem. C **117**, 10636 (2013).
9. Z. Y. Li and Y. Xia, Nano Lett. **10**, 243 (2010).
10. Y. C. Cao, R. Jin, and C. A. Mirkin, Science **297**, 1536 (2002).
11. J. Lin, J. Dellinger, P. Genevet, B. Cluzel, F. de Fornel, and F. Capasso, Phys. Rev. Lett. **109**, 093904 (2012).
12. L. Zhang, A. Kubo, L. Wang, H. Petek, and T. Seideman, J. Phys. Chem. C **117**, 18648 (2013).
13. G. Lerosey, D. F. P. Pile, P. Matheu, G. Bartal, and X. Zhang, Nano Lett. **9**, 327 (2009).
14. A. Baron, E. Devaux, J. C. Rodier, J. P. Hugonin, E. Rousseau, C. Genet, T. W. Ebbesen, and P. Lalanne, Nano Lett. **11**, 4207 (2011).
15. B. Wang and G. P. Wang, Appl. Phys. Lett. **85**, 3599 (2004).
16. C. Ropers, C. C. Neacsu, T. Elsaesser, M. Albrecht, M. B. Raschke, and C. Lienau, Nano Lett. **7**, 2784 (2007).
17. A. G. Curto and F. Javier Garcìa de Abajo, Nano Lett. **8**, 2479 (2008).
18. A. Otto, Z. Phys. **216**, 398 (1968).
19. L. L. Yin, V. K. Vlasko-Vlasov, J. Pearson, J. M. Hiller, J. Hua, U. Welp, D. E. Brown, and C. W. Kimball, Nano Lett. **5**, 1399 (2005).
20. T. Tanemura, K. C. Balram, D. S. Ly-Gagnon, P. Wahl, J. S. White, M. L. Brongersma, and D. A. B. Miller, Nano Lett. **11**, 2693 (2011).
21. I. Dolev, I. Epstein, and A. Arie, Phys. Rev. Lett. **109**, 203903 (2012).
22. Y. H. Chen, J. X. Fu, and Z. Y. Li, Opt. Express **19**, 23908 (2011).
23. Y. H. Chen, L. Huang, L. Gan, and Z. Y. Li, Light Sci. Appl. **1**, e26 (2012).
24. Y. G. Chen, Y. H. Chen, and Z. Y. Li, Opt. Lett. **39**, 339 (2014).
25. Y. G. Chen, F. Y. Yang, J. Liu, and Z. Y. Li, Opt. Express **22**, 14727 (2014).